Engineering Structures 274 (2023) 115114

Contents lists available at ScienceDirect

Engineering Structures

journal homepage: www.elsevier.com/locate/engstruct

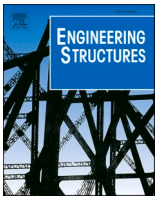

Wind tunnel tests of a hexadecagonal cylinder with imperfections and ancillaries: aerodynamic characterization and technical discussion

Andrea Orlando *, Luisa Pagnini, Maria Pia Repetto

DICCA – Polytechnic School, University of Genoa, Genoa, Italy

ARTICLE INFO

Keywords:
Polygonal cylinder
Wind tunnel tests
Mean force coefficients
Effective Reynolds number
Galloping coefficient

ABSTRACT

This paper evaluates and discusses the aerodynamic properties of a 16-sided polygonal cylinder with imperfections and ancillaries investigated by wind tunnel tests. Two sectional models with different size have been realized, reproducing the peculiarities of real structures, such as the rounded corners, local protuberance due to weld bead, cables, ducts and the external ladder. The models have been subjected to static tests to measure the mean force coefficients and the Strouhal number varying angle of attack, flow velocity, turbulence intensity focusing on the effects of the imperfections and ancillaries on the aerodynamic loads with consideration of Reynolds number effects. The results provide an estimate of the aerodynamic coefficients for this type of elements, quantify the influence of geometrical and flow properties on the aerodynamic behaviour and point out the sensitivity of such polygonal cross-section to galloping instability.

1. Introduction

The flow properties around bluff bodies have attracted extensive research in the last century. The parameters that drive the aerodynamic behaviour of bluff cylinders are the drag coefficient C_D, the lift coefficient C_L and the Strouhal number St, which are closely associated with the vortex shedding dynamics and are evaluated paying special attention to their dependence of Reynolds number, Re.

A vast amount of research has been focused on the flow around stationary circular cylinders; see Roshko [1], Coutanceau & Daefaye [2], Williamson [3,4], Zdravkovich [5], Thompson et al. [6] and Yeung [7] among others. The flow around polygonal cylinders is much less studied. Most of the studies deal with squares and rectangles; significant studies were made by Okajima [8], Igarashi [9], Matsumoto [10], Tamura & Miyagi [11], Breuer et al. [12], Zhou et al. [13], van Hinsberg et al. [14,15]. On the contrary, little attention has been paid in literature to the study of flow around polygonal cylinders with more than 4 sides, even if such sectional shapes are commonly seen in many engineering problems.

Structures like light poles, signal and telecommunication towers (Fig. 1) or wind turbines are mostly characterized by slender polygonal shafts with more than 12 sides, often with the presence of protuberances along the longitudinal axis, such as weld bead, ducts, ladder.

Despite several studies have investigated the aerodynamic loads on real poles and towers [16–18], the specificity of the case studies makes it difficult to generalize the results to other comparable structures. Wind tunnel tests on polygonal cylinders with large edge number are still rare and do not supply reliable benchmark.

Some extensive experimental campaigns about polygonal cylinders with large edge number have been conducted by James [19–21]. He measured the drag coefficient of polygonal sections with 8, 12 and 16 sides as a function of Reynolds number and corner radius, considering 3 different mean directions of the flow. Mehta et al. [22] and Bosch & Guterres [23] carried out wind tunnel tests on octagonal cylinders to verify the drag coefficients proposed by AASHTO for highway support structures [24]. Tian & Li [25] investigated a polygonal cylinder with 24 sides in a low-speed wind tunnel to seek a low drag solution for their prototype supporting frames. Xu et al. [26] systematically studied the wake of polygons with edge number from 3 to 16 through wind tunnel tests, measuring the aerodynamic parameters for two different angles of attack of the wind flow.

There have been attempts to simulate numerically the flow around a polygonal cylinder with more than 4 sides. Tian & Wu [27] calculated the flow field around polygons at the corner orientation for even values of the edge number. Khaledi & Andersson [28] investigated numerically the unsteady wake behind a hexagonal cylinder both corner- and face-oriented.

Two main shortcomings emerge from a review of the research papers

* Corresponding author.
E-mail addresses: andrea.orlando@edu.unige.it (A. Orlando), luisa.pagnini@unige.it (L. Pagnini), repetto@dicca.unige.it (M. Pia Repetto).

https://doi.org/10.1016/j.engstruct.2022.115114
Received 21 March 2022; Received in revised form 15 September 2022; Accepted 9 October 2022
Available online 27 October 2022

dealing with many-sided polygonal cylinders: first, the characterization of the lift coefficient is very poor; second, the study of the flow around polygons is almost entirely limited to one or two main orientations (mean-flow direction aligned with corner or orthogonal to face). Therefore, there is no information about the trend of the aerodynamic coefficients as a function of the flow mean direction and a reliable quantification of the aerodynamic derivatives is almost impossible for such kind of cross-sections.

Due to the lack of information, the engineering design of polygonal cylinders with a high number of edges is often dealt with using information available for circular cylinders, as appears from the analysis of current regulations. The guidelines provided by National Research Council of Italy [29] furnishes the aerodynamic parameters for polygonal shapes up to 12 sides. Sections with higher side number are dealt with as circular. Eurocode 1 [30] does not consider sections with more than 12 sides (e.g., 14 sides) or treat them as circular (e.g., 16 sides). The standard provided by ASCE [31] does not address polygonal sections with more than 8 sides. The current specifications supplied by AASHTO [32] furnish the drag coefficient for 12-sided and 16-sided sections; the proposed values derive from the studies by James [19–21]. ESDU 79,026 [33] provides a method to derive the drag coefficient for sections up to 20 sides, by approximating polygons to circles with an equivalent roughness. On the same principle, ESDU 96,030 [34] supplies St values that apply for both circular and polygonal sections with edge number greater than 8.

These recommendations rely on a polar-symmetry of the cross-section to characterize the aerodynamics of a polygon, thus neglecting some aspects that can become very important in the structural behaviour [35]. First, the provided coefficients are usually referred only to one mean direction of the flow, which is aligned to a symmetry axis of the section (generally the one aligned with a corner). Moreover, the mean lift coefficient, C_L, is always considered to be zero, as well as the lift derivative with respect to the angle of attack, C'_L. Therefore, except in the presence of ice coating [36], mean crosswind buffeting response and galloping instability are not considered by regulations for these kinds of polygonal shafts [37,38]. It is also important to notice that, among the mentioned regulations, only AASHTO and ESDU [32,33] take into account the influence of corner radius on the aerodynamic behaviour of polygonal cylinders with more than 4 sides.

In addition to the described shortages, to the best of the authors' knowledge, the aerodynamic contribution of distributed elements such as the longitudinal weld, cables or the external ladder, which very often recur in poles and tubular towers, is poorly addressed in current regulations and it is analysed by very few scientific papers. Among these, Han et al. [39] tested a static sectional model of a circular light pole with a weld in the wind tunnel. They found that both the aerodynamic forces and the Strouhal number are highly sensitive to the weld position. Nguyen et al. [35] studied the wind-excited response of complex light poles through wind tunnel tests and found out that distributed ancillaries may cause very low critical galloping velocities. A significant research line has addressed the aerodynamic contribution of traffic signals to wind-induced vibrations of their mast-arm support structures [40,41].

Starting from these premises, this paper presents the wind tunnel tests carried out on scale models of a 16-sided polygonal cylinder to investigate its aerodynamic properties focusing on the effects of imperfections and ancillaries, as well as corner radius, with consideration of Reynolds number.

The paper is divided into 6 sections. Section 2 describes the models realized, the wind tunnel facility and the experimental setup used for the tests. Section 3 presents the experimental results on the sectional models, furnishing the aerodynamic coefficients of the 16-sides polygonal cylinder and discussing the effects of Reynolds numbers, corner radius, imperfections and ancillaries. Section 4 adopts the aerodynamic coefficients to analyse possible galloping instability occurrence. Section 5 reports the Strouhal number estimation for the two models in three different orientation. Finally, Section 6 draws the main conclusions and the perspectives for further research.

2. The experimental set-up

A 16-sides polygonal cylinder is reproduced by two sectional models, realized by 3D printing (Fig. 2a), in the following referred to Model A and Model B. They reproduce all the typical geometric features of a real structure obtained with cold-bent steel: the rounded corners, a longitudinal protuberance, representing the presence of weld bead, cables, ice accreting, etc., and the external ladder (Fig. 2b).

Models are 1.8 m long; the diameter is 35 mm (Model A) and 62.5 mm (Model B). The corner radius is equal in both models (3 mm) as it is typical in real structures, due to production processes. Therefore, for model A, the ratio of the radius over the diameter (r/D) is equal to 0.09; for model B it is 0.05. Model surface has been examined by means of a digital microscope. Both models have surface roughness of about 35–40 μm (RMS value); therefore surface roughness to model diameter ratio is $1.1 \bullet 10^{-3}$ for model A and $6.0 \bullet 10^{-4}$ for model B.

Experimental tests have been carried out in the wind tunnel facility

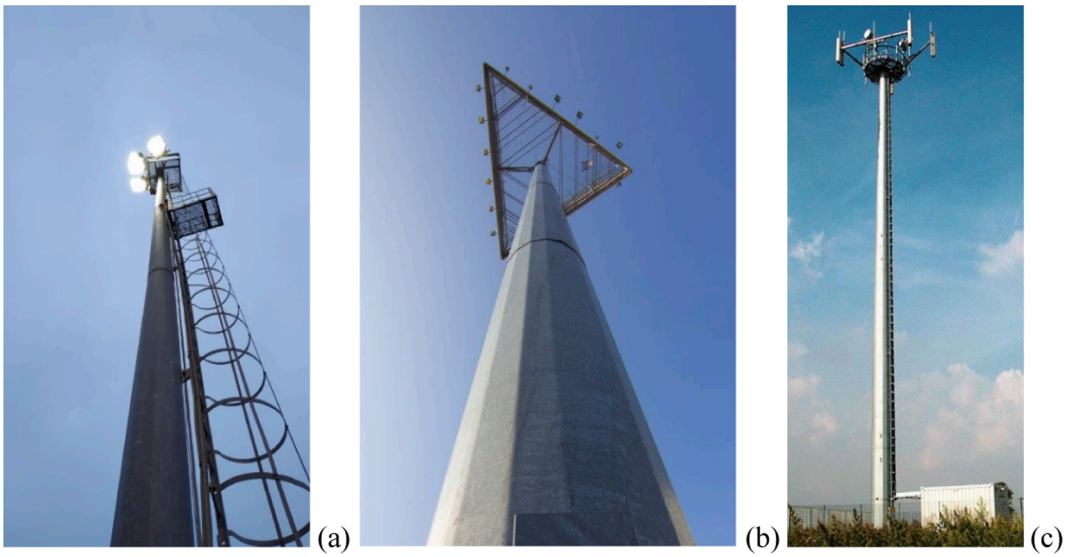

Fig. 1. Examples of 16-sides polygonal shafts in real structures: a) lighting pole; b) signal tower; c) telecommunication tower.

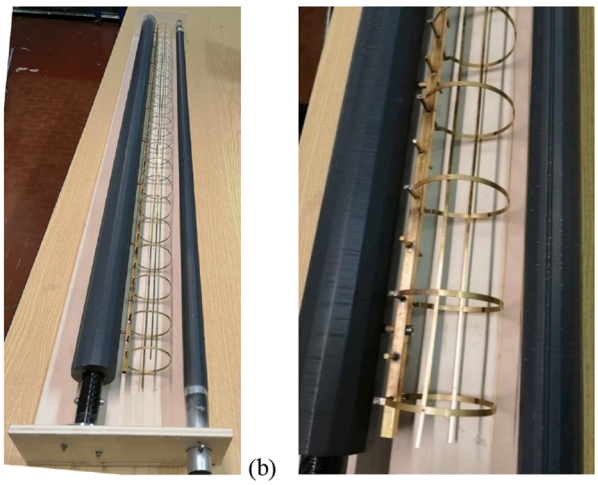

Fig. 2. The wind tunnel sectional models (a), with model B and model A from left to right. Ladder, protuberance and rounded corners in detail (b).

at the Department of Civil, Chemical and Environmental Engineering of the Polytechnic School of the University of Genoa. It is a closed-loop subsonic wind tunnel for aerodynamic and civil experiments, with working section 1.7 m (width) × 1.35 m (height) and length 8.8 m, with a 1.3 m diameter turntable. It is equipped with a pitot tube to measure the undisturbed wind speed (placed 0.25 m below the wind tunnel roof, outside the wall boundary layer) and a fast-response multi-hole probe (Cobra probe) managed through a robotic arm to measure wind velocity profiles and wake properties. Flow uniformity is below 1 % and longitudinal turbulence intensity I_u is below 0.2 % in smooth flow conditions. Blockage ratio is 4.6 % for model B and 2.6 % for model A; therefore, no corrections have been applied to the measurements.

Both a dense and a sparse grid consisting of wooden square bars have been used to test the sectional models in smooth and in turbulent flow (Fig. 3). Placing the grids upstream of the model, two turbulence levels have been generated at the test section, characterized by I_u equal to 7.5 % and 3.5 %, respectively, and integral length scale L_u equal to 50 mm and 25 mm.

The experimental campaign has been divided into three sets of tests, each one with a different objective. They are summarised in Table 1. The definition of the angle of attack of the flow with respect to the sectional models is shown in Fig. 4, both in the case without (4a) and with (4b) the ladder. It is timely to note that $\alpha = 11.25^\circ$ identifies a symmetry axis of the configuration for the bare cylinder as the protuberance is aligned with this direction..

The first set of tests (Set n°1) aims to investigate the aerodynamic behaviour of the hexadecagonal cross-section without ancillaries. Considering the symmetry of the section, the investigated sector is $0^\circ - 22.5^\circ$ (Fig. 4a), starting and ending with the mean flow direction perpendicular to a face of the model. Flow directions have been investigated at 2° increments except in the neighbourhood of the corner, where a more refined 1.25° step has been used. Both sectional models have been tested in smooth and in turbulent flow conditions, varying the mean flow velocity from about 11 to 22 m/s; the Re number is in the range $3 \bullet 10^4$: 10^5. In these experiments, the imperfection lies on the leeward side and it is assumed that it does not affect the results.

The second run of tests (Set n°2) investigates the contribution of the protuberance, varying the angle of attack from 0° to 360° at 5.625° increments. In this case, tests have been carried out on model B at different turbulence levels; wind velocity varies between 11.1 and 13.6 m/s due to the presence of the grid.

The third testing set (Set n°3) investigates the model (Model B) equipped with the ladder. The angle of attack has been varied from 0° to 360° in steps of 11.25°. Tests have been carried out in smooth flow at 13.6 m/s.

The aerodynamic forces on sectional models have been measured by two quartz six-component dynamometers at either end of the model. The force balances are mounted on two high precision stepper motors rotating the model automatically with 0.05° sensitivity (Fig. 5). The stepper motors are in turn connected to a steel frame, bolted to the concrete floor slab, which acts to eliminate the flow-induced cylinder vibrations. In the static setup, the test cylinder spans the entire width of the test chamber preventing three-dimensional effects due to finite aspect ratio.

For each test run, the mean aerodynamic force coefficients have been evaluated as:

$$C_i = \frac{\overline{F}_i}{\frac{1}{2}\rho \bar{u}^2 A_{ref}} \quad i = D, L \tag{1}$$

where $\bar{u}$ is the reference mean wind velocity (time average of the pitot measure), A_{ref} is the reference area of the model (model diameter × tunnel width), ρ is the air density and $\overline{F}_D$,$\overline{F}_L$ are the time average of the aerodynamic force acting in the longitudinal and lateral direction (Fig. 4), respectively.

The duration of each test is 60 s. The transducer measurement signals are sampled at 2 kHz.

3. Experimental aerodynamic coefficients

3.1. Role of the angle of attack

This section discusses the aerodynamic coefficients of the 16-sides polygonal cylinder, considering the results of test set n°1 obtained on model B, exploring the sector $\alpha = 0{:}22.5^\circ$, being $\alpha = 11.25^\circ$ the symmetrical configuration where the corner is aligned with the mean flow

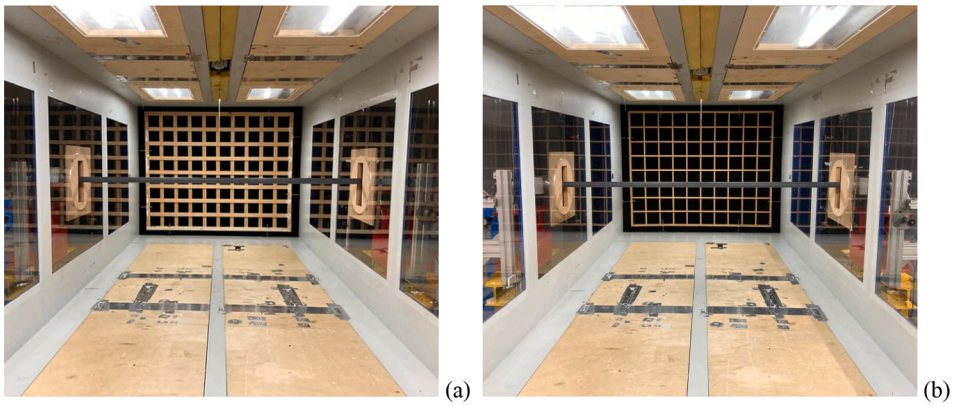

Fig. 3. Wind tunnel inside-view with turbulent flow conditions. Dense grid (a) and sparse grid (b).

Table 1
Wind tunnel tests on the sectional models.

Set number	Angles of attack α (°)	Turbulence Intensity I_u (%)	Flow speed (m/s)	r/D	Protuberance	Ladder
1	0:2:10,11.25,12.5:2:22.5	0.2,3.5,7.5	11.1:22.1	0.05,0.09	No	No
2	0:5.625:360	0.2,3.5,7.5	11.1:13.6	0.05	Yes	No
3	0:11.25:360	0.2	13.6	0.05	Yes	Yes

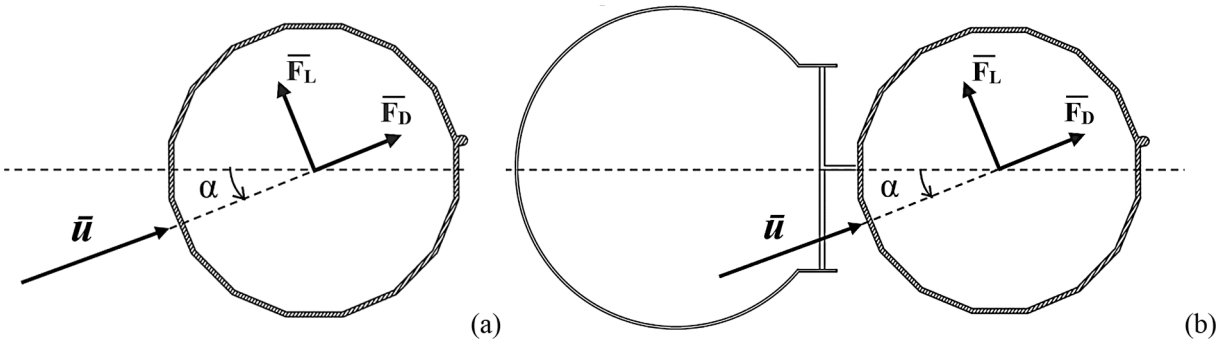

Fig. 4. Sketches of the sectional models, without (a) and with (b) the ladder, with direction of mean inflow and mean aerodynamic forces. In the figure, α = 22.5°.

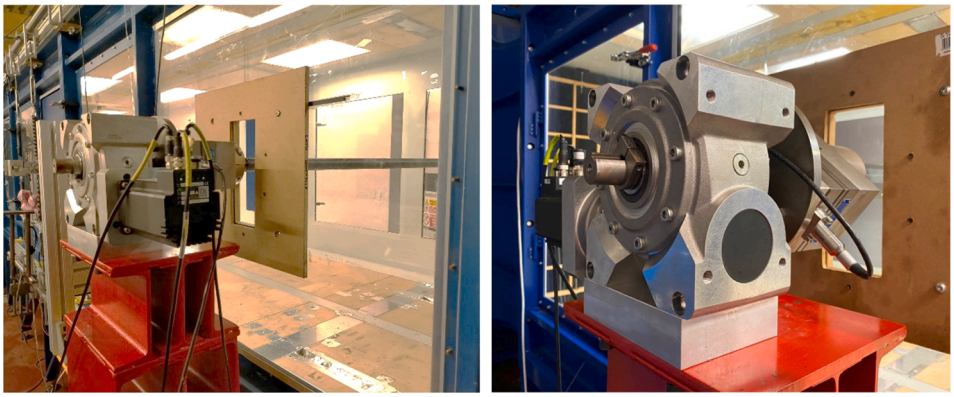

Fig. 5. Force balances on stepper motor to test the sectional models.

direction. At α = 0° and α = 22.5° the mean flow direction is perpendicular to a side of the cross-section.

Fig. 6a plots the drag coefficient obtained in smooth flow (I_u < 0.2 %), on varying the angle of attack, at four different wind speeds, i.e., four different Re, ranging from 5.6 10^4 (black line) to 9.1•10^4 (light grey line). In the figure, the red dashed line shows the symmetry axis of the model at α = 11.25°; the sketches help to understand the incidence of the flow with respect to the sides or corners of the bare cylinder. The obtained drag coefficients are always lower than 1.2, with maximum value of 1.12 at α = 0° at the lowest investigated Re value. The variation with α is moderate: the drag undergoes an overall 15 % variation at Re = 5.6 10^4 and a 25 % overall variation at Re = 9.1 10^4. The apparent variation with Re suggests that, increasing flow velocity, the cylinder is entering the critical regime characterized by the drag crisis. Indeed, for every angle of attack, the drag at Re = 9.1 10^4 reduces by 40–50 % with respect to the case Re = 5.6•10^4.

Consistently with the physical symmetry of the model, the drag coefficient has an almost symmetric trend. Slight asymmetries, increasing at high Re, can be justified by the instability that characterises the critical regime, where even very small irregularities or deviations from the ideal configuration can result in huge variations of aerodynamic coefficients.

Fig. 6b plots the lift coefficients, under the same conditions and with the same convention already described. The four plots converge to zero at α = 11.25°, which is the symmetric configuration where the corner is

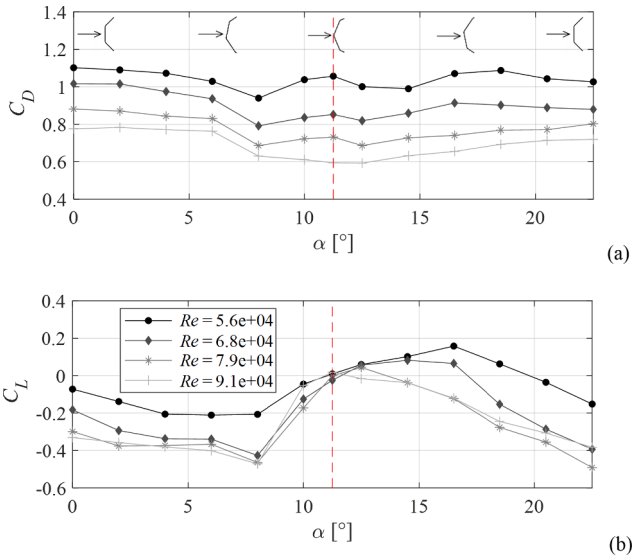

Fig. 6. Mean drag (a) and lift (b) coefficients of hexadecagonal shape as a function of the angle of attack, in smooth flow (I_u < 0.2 %) and different mean flow velocities. Corner radius r/D = 0.05.

aligned with the mean flow direction. At $\alpha = 0°$ and $\alpha = 22.5°$, where the mean flow direction is perpendicular to a side of the cross-section, the lift assumes a considerable negative value, despite the theoretical symmetry of this layout. This phenomenon appears rather unexpected, and might be due to the instability of the wake that could be very sensitive to slight irregularities of the corners or to slight deviations of the flow.

Notable results concern maximum and minimum lift values obtained in the investigated ranges. Despite being neglected by current standards, the lift coefficient assumes remarkable positive and negative values, up to the 40 % of the drag, confirming the results obtained by James [20]. At the lowest flow velocity, the lift curve is fairly skew-symmetric (except the last two values, at 20° and 22.5°), and its maximum and minimum values are located halfway (i.e., $\alpha = 6.125°$) between the two symmetric configurations (corner-orientation and face-orientation). Increasing the wind velocity and Reynolds number, the lift curve gradually deviates from the expected skew-symmetrical trend, lowering as velocity increases. In addition, the maximum and minimum lift occurs closer to the corner configuration. This result proves the high instability of this coefficient that can be related to the onset of the critical regime in smooth flow conditions, coherently with what suggested by Fig. 6a.

Fig. 7 shows the drag (a) and lift (b) coefficients measured on model B on varying the angle of attack, at three different turbulence intensity values, corresponding to 0.2 % (black line), 3.5 % (grey line) and 7.5 % (light grey line). Tests are carried out at $Re = 5.6\ 10^4$ in smooth flow. The presence of the grid causes a slight decrease in the flow mean speed and Re, which is reduced by 10 % with the sparse grid ($I_u = 3.5$ %) and by 20 % with the dense one ($I_u = 7.5$ %). Therefore the three curves in Fig. 7 are obtained respectively at $Re = 5.6 \bullet 10^4$, $5.1 \bullet 10^4$ and $4.5 \bullet 10^4$.

Fig. 7a shows that drag coefficient considerably decreases as turbulence increases, in agreement with what is reported in ESDU 79,026 [33], where this behaviour is addressed by the so-called effective Reynolds number (Section 3.3).

Fig. 7b shows that turbulence plays a very important role also on the lift coefficient, as it gives rise to a change of sign for almost every direction of the flow. It is also interesting to note that, when entering in the critical range, the three lift curves are still almost skew-symmetrical (differently from Fig. 6b) except for the last two angles, $\alpha = 20.5°$, 22.5°. This suggests the presence of some small irregularities around the direction $\alpha = 22.5°$, which take on greater significance in the critical range. Further investigations will be carried out in section 3.3.

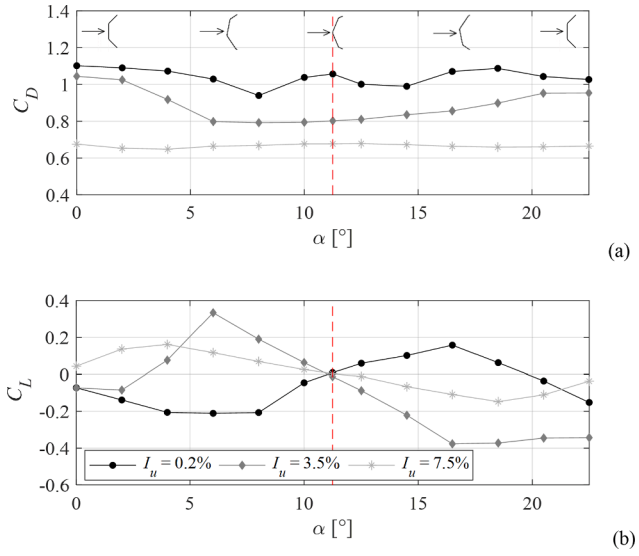

Fig. 7. Mean drag (a) and lift (b) coefficients of hexadecagonal shape as a function of the angle of attack, with Re ranging from $4.5 \bullet 10^4$ to $5.6 \bullet 10^4$ and different turbulence intensities. Corner radius r/D = 0.05.

3.2. Role of corner radius

The role of the corner radius, r, has been investigated by comparing the results obtained on model A (r/D = 0.09) and model B (r/D = 0.05). Fig. 8 shows the drag (a) and lift (b) coefficients obtained in smooth flow, setting two flow velocities that supply very close Reynolds number ($Re = 5.2 \bullet 10^4$ for model A and $Re = 5.6 \bullet 10^4$ for model B) and subcritical range.

The increase of corner radius makes the cross-section closer to a circle from an aerodynamic viewpoint, regularizing the trend of both drag and lift coefficients. In particular, the drag coefficient shows a slight increase, while the lift coefficient approaches to zero, and becomes zero in the three symmetry configurations, i.e., $\alpha = 0°$, $\alpha = 11.25°$, $\alpha = 22.5°$. Considering that the weld is more pronounced in the small model (Model A), the results suggest that the negative lift of the large model (Model B) at face-orientation should not be ascribed to the presence of the longitudinal weld along the cylinder. This confirms that in the test set n ° 1 the role of the leeward protuberance is negligible.

3.3. Role of Reynolds number

This section analyses the role of Reynolds number in the aerodynamic behaviour of the *hexa*-decagonal cross-section. Results obtained on both the large (Model B) and the small (Model A) model, as well as tests in smooth flow and at the two considered turbulence levels are reported on the same diagrams.

Following the procedure described by ESDU 79,026 [33], the effect of turbulence on variation of C_D with Re is considered by multiplying Reynolds number by a factor f_T dependent on the turbulence properties of the approaching flow. This factor is produced using empirical correlations (provided in graphic form) in which the force coefficient for a multi-sided polygon is related to an equivalent force coefficient for a rough circular cylinder. Roughness of the equivalent circular cylinder is evaluated based on side number and corner radius of the polygon, assuming that its surface is smooth. No guidance is provided for polygonal cylinders with rough surface.

Results are then presented both as a function of Reynolds number Re and effective Reynolds number f_T Re. In smooth flow, $f_T = 1$ and the effective Reynolds number coincides with Re.

Figs. 9-10 show the Reynolds effect on drag and lift force coefficient, respectively. Three main configurations are investigated: face-

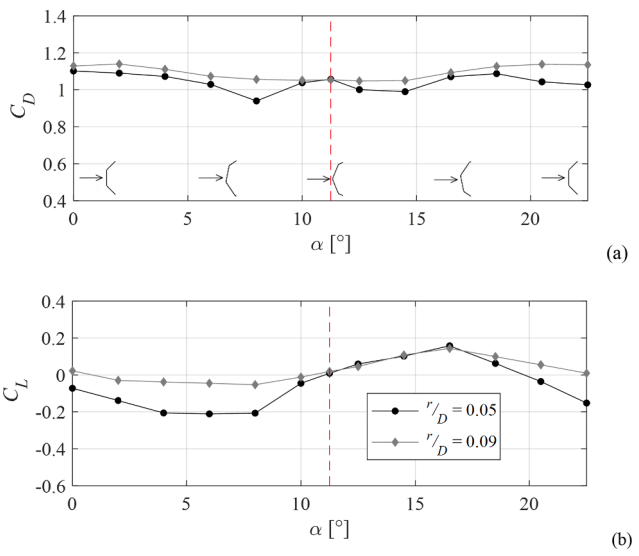

Fig. 8. Mean drag (a) and lift (b) coefficients of hexadecagonal shape as a function of the angle of attack, with smooth flow ($I_u < 0.2$ %) and different corner radius. $Re = 5.2 \bullet 10^4$ and $5.6 \bullet 10^4$.

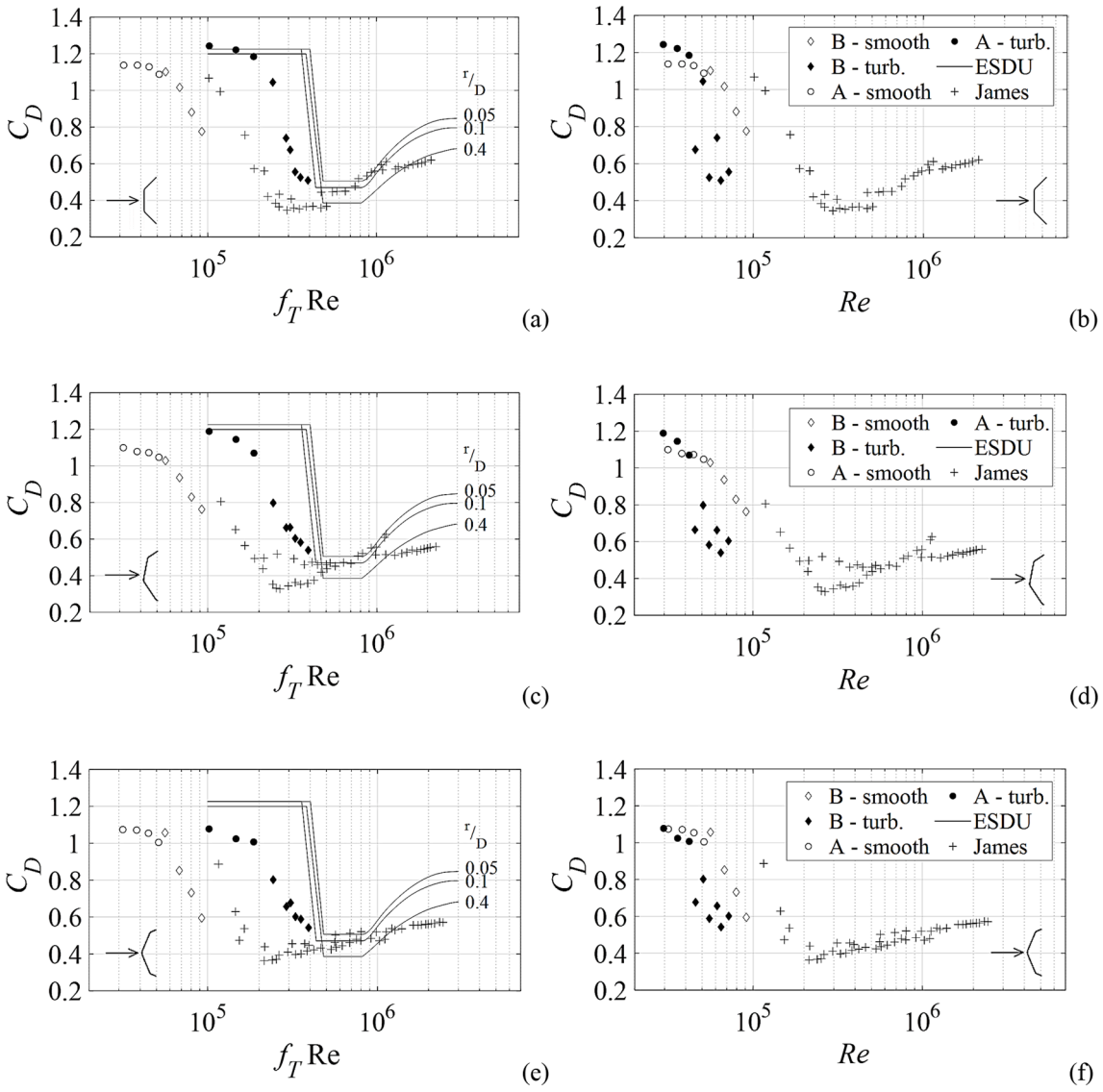

Fig. 9. Mean drag coefficient of hexadecagonal shape as a function of effective Reynolds number (a, c, e) and as a function of Reynolds number (b, d, f). The angle of attack of the flow is α = 0° (a, b), α = 6° (c, d), α = 11.25° (e, f).

orientation (α = 0°, Fig. 10a, 10b, 11a, 11b), corner-orientation (α = 11.25°, Fig. 10e, 10f, 11e, 11f) and an intermediate one (α = 6°, Fig. 10c, 10d, 11c, 11d).

In Fig. 9, the measured drag coefficients of the present campaign are compared with significant results reported by James [20], who investigated the same three orientations, therefore supplying a valuable reference for this investigation. Coefficients provided by James were obtained in smooth flow (even if the flow characterization is not supplied by the author), at fixed corner radius (r/D = 0.12) and with surface roughness to model diameter ratio ranging from $0.83 \bullet 10^{-5}$ to $3.3 \bullet 10^{-5}$.

Values proposed by ESDU 79,026 for the hexadecagonal shape are also included in the figure in the form of a parametric curve for different values of r/D. This is a conservative curve drawn from James' investigations to be used by structural designers independently of the orientation of the cylinder. ESDU also suggests that the corner-orientation (α = 11.25°) produces the maximum aerodynamic forces. However, this seems not supported by experimental results shown in the figure, where drag coefficient at α = 6° and especially at α = 12.5° is slightly lower than the values at α = 0°, showing that the face-orientation produces the maximum drag force, as it was found also by James.

For every model orientation, the drag reduction measured in smooth flow is consistent with results by James, even if only the first part of the critical range is addressed by our tests. However, there is a clear offset between the two trends: the drag crisis observed in the current study occurs at lower Re number than the reference study. This effect can be due to the higher surface roughness of the models adopted in the present campaign ($0.6{:}1.1 \bullet 10^{-3}$ versus $0.83{:}3.3 \bullet 10^{-5}$). Indeed, as pointed out in several studies [20,42,43], increasing surface roughness to model size shifts the C_D vs Re curve up and to the left. The same effect, especially for face-orientation, is observed when comparing results of the current study in turbulent flow with the provisions by ESDU, which refer to smooth cylinders.

The most impressive result emerging from Fig. 9a, 10c, 10e is a clear separation into two branches between turbulent (full symbols) and smooth tests (void symbols). Turbulent-flow results are translated in a separate Reynolds range because f_T assumes values up to 7 in the examined turbulent conditions. However, if we present the results as a function of Re, data in the different flow regimes get closer but lose some alignment (Fig. 10b, 10d, 10f). Therefore, these findings suggest that the curve proposed by ESDU is a good approximation for turbulent flow conditions, while it can lead to strong overestimation of the

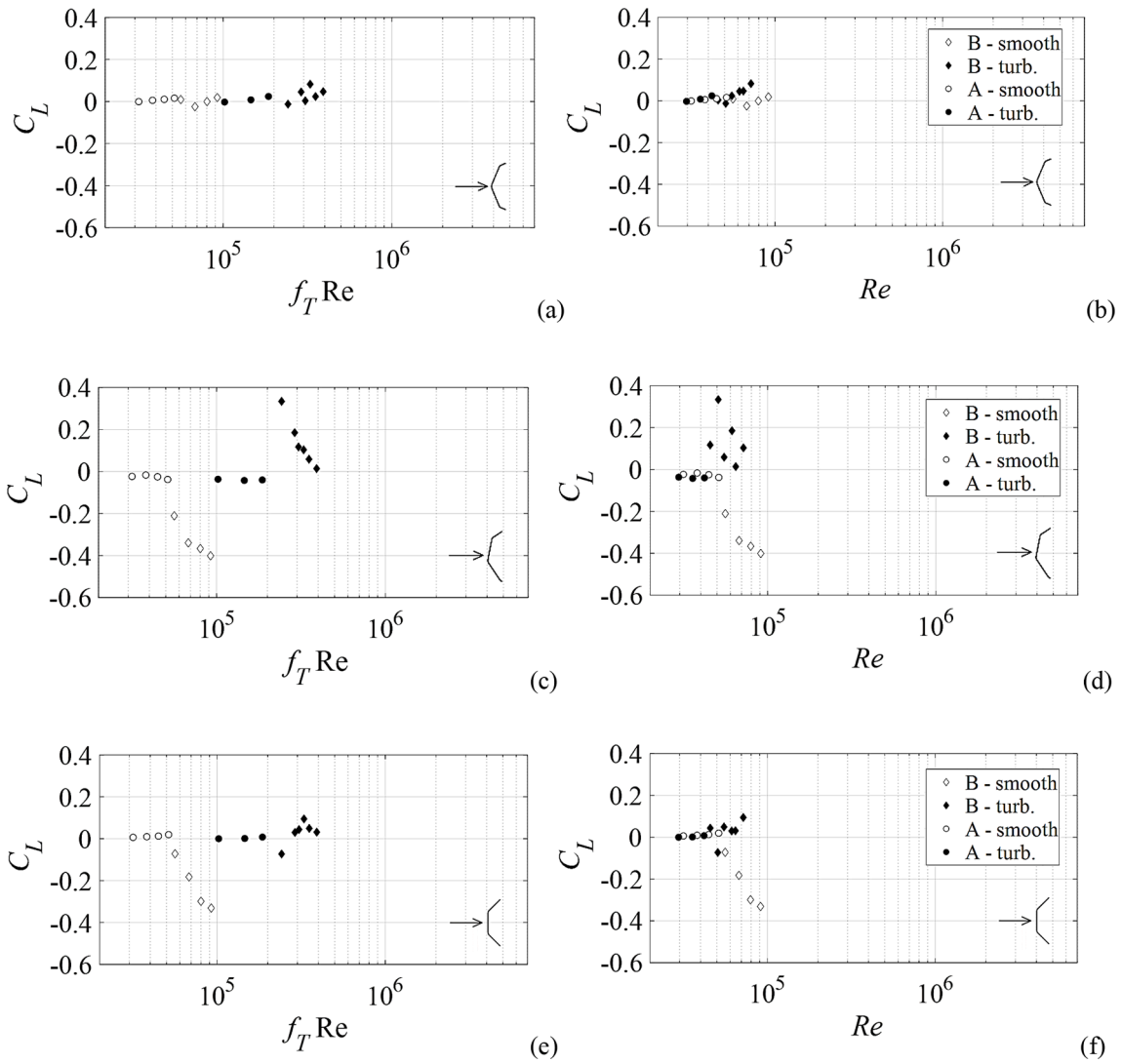

Fig. 10. Mean lift coefficient of hexadecagonal shape as a function of effective Reynolds number (a, c, e) and as a function of Reynolds number (b, d, f). The angle of attack of the flow is α = 11.25° (a, b), α = 6° (c, d), α = 0° (e, f).

aerodynamic loads in smooth flow. Above all, it suggests that the definition of an effective Reynolds number for the prediction of the drag coefficient is a very promising tool and should be further studied and refined.

In Fig. 10, the lift coefficients measured on the two models (circles and diamonds for model A and B, respectively) highlight that the change of shape changes completely the extent of the transversal force.

At corner orientation (α = 11.25°, Fig. 10a, b), the lift coefficient is essentially zero regardless of Reynolds number. As already mentioned, this result proves that the theoretical symmetry of the configuration is well reproduced by both models. At the mid-orientation (α = 6°, Fig. 10c, 10d), the model is asymmetrical with respect to the flow and thus the lift force reaches its maximum magnitude among the three considered configurations, both for model A ($C_L \approx 0.05$) and model B ($C_L \approx 0.4$). At face-orientation (α = 0°, Fig. 10e, 10f), values obtained on model A recall the trend of the corner-orientation, while model B undergoes a considerable lift force. Considering the theoretical symmetry of this configuration, one possible explanation is that some unavoidable irregularities affect the symmetry of model B. The effect of the asymmetries, both intrinsic of the orientation or due to slight irregularities, is amplified in the critical regime; indeed for each orientation the maximum lift is reached in the middle of the critical range of Re.

The lift evolves non-monotonically along with f_TRe, with an abrupt change of sign in the transition from smooth to turbulent flow. Actually, it happens that the position of the horizontal bars of the grid adopted in the wind tunnel to produce turbulence is not perfectly aligned with the model position, generating possible inhomogeneity between the flow above and below it. This condition is likely to reverse the lift sign, showing again the high instability of the critical regime. This effect is significant of what may occur also in full-scale conditions, when several perturbations (from obstacles, trees, etc.) affect the direction of the flow.

3.4. Role of the protuberance

The contribution of a local protuberance to the aerodynamic behaviour of the cylinder is investigated in the second run of tests (Set n°2), where model B has been tested varying the angle of attack from 0° to 360°.

Fig. 11 reports the drag (a) and lift (b) coefficients on varying the angle of attack. The conditions of flow aligned with the symmetry axis of the cross-section, crossing the protuberance, is highlighted by a vertical red dashed line. Consistently with the results previously presented, the figure shows a good symmetry and skew-symmetry in C_D and C_L, respectively, as well as a decreasing trend of the drag coefficient along with the increase of the Reynolds number.

The fluctuating trend of the aerodynamic lift coefficient appears

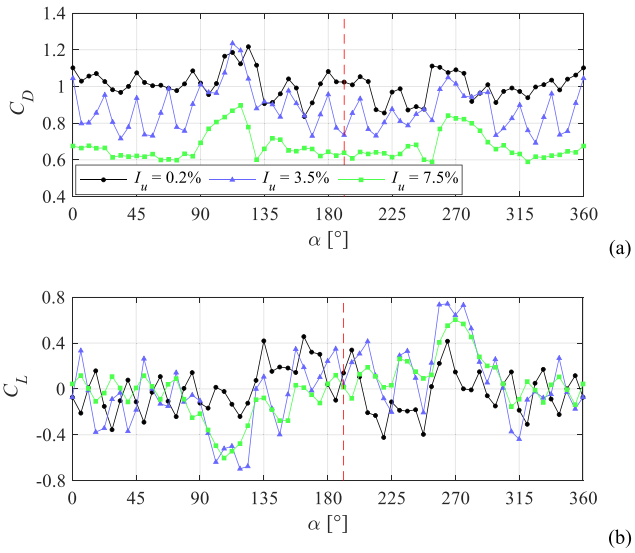

Fig. 11. Mean drag (a) and lift (b) coefficients of hexadecagonal shape with local protuberance as a function of the angle of attack, with Re ranging from $4.5\bullet10^4$ to $5.6\bullet10^4$ and different turbulence intensities. Corner radius r/D = 0.05.

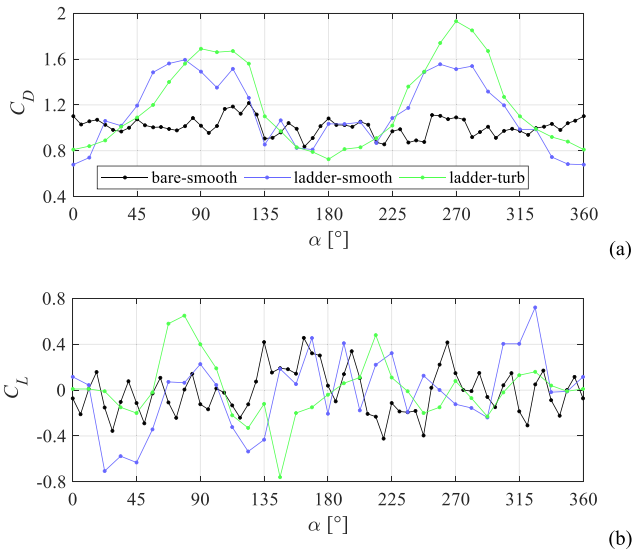

Fig. 12. Mean drag (a) and lift (b) coefficients as a function of the angle of attack, in smooth (I_u = 0.2 %) and in turbulent flow (I_u = 7.5 %), with and without the ladder. Corner radius r/D = 0.05, Re ranging from $4.5\bullet10^4$ to $5.6\bullet10^4$.

typical of multisided cylinders. The slopes of C_L with respect to the angle of attack are negative for flat orientation and positive for corner orientation [41,44]. The figure also shows that the protuberance affects considerably the diagram around α = 110° and 270°, where it lies on an axis of the cross-section almost orthogonal to the flow direction. In this condition, besides increasing the exposed area (therefore increasing the overall drag), it enhances the asymmetry of the section with respect to the flow (increasing the modulus of the lift) causing a significant increase of the drag coefficient (+50 % with respect to the bare cylinder) and especially of the lift modulus, that almost reaches 0.8 in turbulent flow.

The intermediate turbulence level, which falls in the middle of the critical range of f_TRe, produces the most unstable trend of both coefficients, causing in particular the highest values of the lift. In addition, the presence of the grid for producing turbulence makes the lift change sign for all the directions where the weld has a moderate effect, extending the results presented in Section 3.3 to the whole directional domain.

3.5. Role of the ladder

The presence of ladder prevents the cross-section from having any symmetry (Fig. 4b); therefore, the study of the cylinder equipped with this ancillary is carried out for α = 0:360°. Fig. 12 shows drag (a) and lift (b) coefficients of the cylinder with (blue line) and without (black line) ladder in smooth flow, and with the ladder in turbulent flow (green line). It is important to remind that, consistently with Eq. (1), aerodynamic coefficients are obtained dividing by the reference area of the bare polygonal cylinder even when the ancillary is present.

The ladder produces different effects on the drag coefficient at different angles of attack. When it has the maximum exposition (around α = 90° and α = 270°), the drag increases, from an approximately unitary value on average up to 1.6 and 2 respectively in smooth and turbulent conditions. On the contrary, when the ladder is upstream, it produces a sort of equivalent Reynolds effect, reducing C_D to about 0.8.

Besides increasing the drag, the ladder has the effect of augmenting the maximum and minimum values of the lift when it is on a sectional axis skewed with respect to the wind direction.

In the neighbourhood of α = 180°, both coefficients almost overlap those measured on the bare cylinder, as the ladder is shaded by the shaft.

Notwithstanding the very fluctuating trend of C_L shown in Fig. 12b, tests have shown a good repeatability, even it is likely that this trend is very sensitive to test flow and small shape irregularities.

To appreciate the real contribution of this evaluation in the structural design, diagram in Fig. 13 compares measured drag values with a typical evaluation from current regulations. According to current standards, aerodynamic coefficients of the shaft and of the ladder can be calculated separately and summed to obtain a global aerodynamic coefficient of the ensemble. By following this method, values represented by the green line are obtained by summing the drag coefficients of the shaft and of the ladder provided by the Italian guidelines [29]. The black line represents values obtained by summing the drag coefficient of the ladder provided by the Italian standard to the drag coefficient found experimentally on the bare cylinder. The blue line indicates the drag coefficients measured on the ensemble (cylinder + ladder), as in Fig. 12a.

The reported outcomes suggest some important aspects that should be taken into account in the design of these kind of structures to wind actions. For wind direction aligned with the ladder (α = 0°), the shaft is shaded and the measured drag coefficient is reduced, while it is strongly overestimated by the standard calculation. For wind directions opposite to the ladder (α = 180°), the ladder is shaded and the pole actually behaves like a bare cylinder, with a good agreement between tested and standard calculated drag coefficients. For directions orthogonal to the ancillary (around α = 90° and α = 270°), the ladder has the maximum

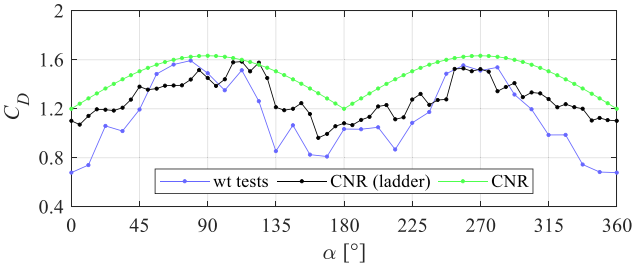

Fig. 13. Mean drag coefficient as a function of the angle of attack, with smooth flow (I_u < 0.2 %) and Re ranging from $4.5\bullet10^4$ to $5.6\bullet10^4$. Corner radius r/D = 0.05. The ladder and the shaft are considered from measurements and from the Italian guidelines [29].

exposition and again the standard calculations are able to provide a reliable quantification of the aerodynamic contribution to drag. For other skewed directions (α ranging from about 120° to 240°), it is difficult to predict the aerodynamic contribution of the ladder, which is able to modify deeply the drag even without changing the exposed area.

4. Galloping investigation

The possible occurrence of galloping instability is investigated by calculating the galloping coefficient a_G:

$$a_G = -(C_D + C'_L) \tag{2}$$

where C'_L is the first derivative of the lift coefficient with respect to the angle of attack, expressed in radians. The necessary condition for galloping instability occurrence, known as the Glauert-Den Hartog criterion, is a_G greater than 0, i.e., $C_D + C'_L < 0$. According to the formulation [45] a_G is inversely proportional to the critical velocity, so the larger a_G, the lower the critical wind velocity from which the instability may occur. ′

In this study, the galloping coefficient is computed using the measurements of C_D and C_L and calculating the lift derivative through the symmetric difference quotient:

$$C'_L(\alpha_i) = \frac{C_L(\alpha_{i+1}) - C_L(\alpha_{i-1})}{\alpha_{i+1} - \alpha_{i-1}} \tag{3}$$

where α_i is the i-th angle of attack investigated in the wind tunnel test.

Fig. 14 shows the quantity $C_D + C'_L$ of the bare cylinder (Model B) as a function of α, measured at wind velocity 13.6 m/s and Re = 5.6 10^4 in smooth flow, Re = 5.1•10^4 and 4.5•10^4 in turbulent flow (I_u = 3.5 % and 7.5 % respectively). Fig. 14a shows results in the sector α = 0:22.5°, with step not larger than 2°; Fig. 14 b investigates the whole domain α = 0:360° at 5.625° increments.

From a theoretical viewpoint, being the galloping coefficient the sum of a symmetric function of α (C_D) with the derivative of a skew-symmetric one (C'_L), the galloping coefficient of the sector α = 0:22.5° should have a symmetric trend. The diagram in Fig. 14a shows a good general symmetry, even with some unavoidable discrepancies.

Measurements obtained at the intermediate turbulence level (I_u = 3.5 %) supply the largest a_G, due to the large angular variations of the lift measured at that flow condition. Increasing furtherly I_u, a_G approaches to zero. It is also worth noting that values obtained in smooth and turbulent flow are often of opposite sign, thus, for each considered direction α, there exists a flow condition in which the instability condition is met. It means that, for this particular polygonal section, several wind directions can potentially generate a galloping phenomenon.

Considering the whole domain α = 0:360°, Fig. 14b shows that, fixed a turbulence level, the condition $a_G < 0$ is satisfied frequently; however, the most critical sector actually seems to be 0:22.5° (where the influence of the weld is quite irrelevant).

It should be underlined that values reported are affected by unavoidable uncertainties arising from the sensitivity and accuracy of the instruments used and from the discretization of the measured values. A characterization of these uncertainties is reported in [46]. However, considering the small variations of the drag and the Lagrange's mean value theorem, the values computed in Fig. 14b are representative of at least one point inside the 11.25°-wide neighborhood of each reported value. This is supported by Fig. 14a, that supplies densely sampled data for the first angular sector, with values completely consistent with Fig. 14b.

Downstream of this discussion, these results intend to highlight, beyond the numerical values, the possible sensitivity of this kind of polygonal shapes to aeroelastic instabilities [37].

Fig. 15 compares galloping coefficients of model A (r/D = 0.09, grey line) and B (r/D = 0,05, black line) in smooth flow, highlighting a general flattening of the diagram at positive values with the increase of r/D, as the aerodynamic behaviour of the polygon tends to that of a circular cylinder (as discussed in section 3.2, Fig. 8).

Fig. 16 highlights the influence of the ladder on a_G, comparing results of model B with (grey line) and without (black line) ladder in smooth flow. The ladder increases the regularity of $C_D + C'_L$, which becomes positive for all directions except for a very small sector, where the ladder is upstream and produces a severe decrease of the drag (Fig. 12a). From a technical point of view, beyond the specific typology of the ancillary investigated, the presence of the ladder can be interpreted as an increase in flow irregularity, comparable to a presence of higher turbulence in the flow around the body. In these conditions, typically the classic galloping phenomenon, in quasi-steady approach, is less likely, exactly as pointed out in Fig. 1.

5. Strouhal number

The Strouhal number St links the vortex shedding frequency f_s with the mean flow velocity ū, according to the relationship:

$$St = \frac{f_s D}{\bar{u}} \tag{4}$$

where ū is the reference mean wind velocity, D is model diameter, f_s is the vortex shedding frequency.

Fig. 17 shows the power spectral density (PSD) function of the lift force measured on model B in smooth flow with ū=13.6 m/s (Fig. 17a)

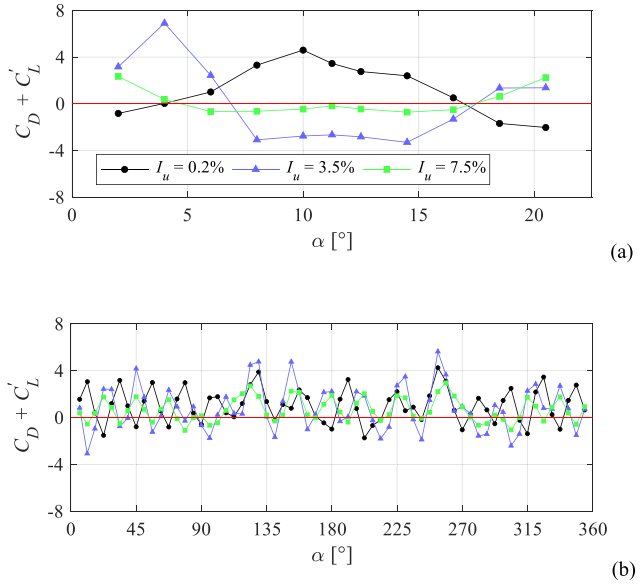

Fig. 14. Galloping coefficient as a function of the angle of attack, Re ranging from 4.5•10^4 to 5.6•10^4 and different turbulence intensities. Corner radius r/D = 0.05. Considered directional domain: 0–22.5° (a) and 0-360° (b).

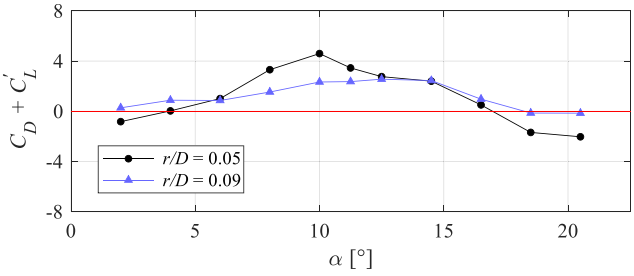

Fig. 15. Galloping coefficient as a function of the angle of attack, Re ranging from 4.5•10^4 to 5.6•10^4 and fixed turbulence intensity (0.2%), varying corner radius.

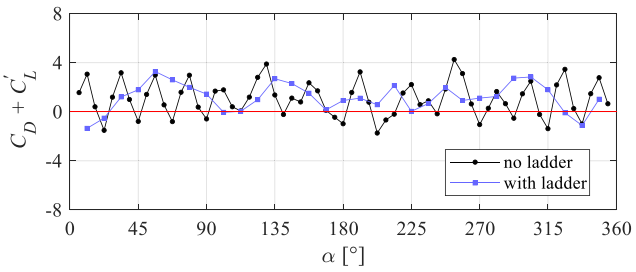

Fig. 16. Galloping coefficient as a function of the angle of attack, Re ranging from $4.5 \bullet 10^4$ to $5.6 \bullet 10^4$ and fixed turbulence intensity (0.2%), with and without the ladder.

and in turbulent flow (I_u = 7.5 %) with ū=19.3 m/s (Fig. 17b). In the Figure, vertical grey line identifies the model frequencies, vertical black line singles out the value of the vortex shedding frequency that changes with flow velocity.

The comparison between the two diagrams highlights the role of turbulence that is able to suppress the vortex shedding excitation, whose energy content (Fig. 17b) is about 20 times lower than in smooth flow (Fig. 17a).

The Strouhal number of the hexadecagonal cross-section has been studied as a function of Reynolds number for the three main orientations of the model.

Fig. 18 shows St evaluated from the tests on both model A and B, both in smooth flow and with the two turbulence levels, as well as for every considered flow velocity. Three main configurations are investigated: face-orientation (α = 0°, Fig. 18a), intermediate orientation (α = 6°, Fig. 18b) and corner-orientation (α = 11.25°, Fig. 18c). Results are compared with investigations carried out by ESDU 96,030 [34] for cylinders with circular or polygonal cross-section (side number greater than 8). ESDU considers polygons as circles characterized by an equivalent roughness based on edge number and corner radius. The document provides the diagram of St as a function of the effective Reynolds number, valid for every circular or polygonal section. According to this provision, the asymptotic decrease at high Re depends on the roughness ε/D of the section, real (for circles) or calculated in equivalent terms (for polygons). However, it is timely to stress that the values of ε/D considered in ESDU 96,030 are actually useful for applications with circular sections. Values of ε/D typical of polygonal sections are usually higher than the values investigated by ESDU. Moreover, as in the case of the drag coefficient, ESDU refers only to polygons corner-oriented.

The results suggest, from a qualitative viewpoint, some considerations already discussed for the mean force coefficients. In particular, smooth and turbulent values follow a similar trend in different domain of f_TRe. With regard to the face-orientation, the turbulent values follow the trend proposed by ESDU, but at a lower f_TRe.

If we move to the corner-orientation, three main differences are noted. First, the subcritical smooth values stabilize at a lower St with respect to the face orientation. Second, the sudden growth, both for turbulent and smooth values, seems to occur earlier than the first orientation, at lower f_TRe. Last, the St values obtained in turbulent conditions scatter across the critical Reynolds range, following two different branches for the two models tested.

Analysing the diagram referred to the mid orientation (α = 6°), intermediate results are obtained, both with regard to the subcritical St and with respect to the scattering of the critical values, suggesting a monotonic evolution of the aerodynamic behaviour changing the mean flow direction. It is timely to observe that, unfortunately, the Reynolds range covered in the present campaign is quite low to characterize the asymptotic decrease of St, where differences between circular and polygonal sections should arise.

6. Conclusions and perspectives

Driven by the lack of knowledge about the aerodynamic properties of polygonal cylinders, the paper discusses the results of the wind tunnel tests carried out on hexadecagonal shaped sectional models that are commonly used in slender structures such as lighting poles, signal tower, antenna masts as well as wind turbines, paying particular attention to the role of imperfections and ancillaries on the aerodynamic load. The investigated models reproduce the peculiarities of real structures, such as protuberances produced by the weld bead, ducts, the external ladder and also rounded corners. Static tests have been performed to measure the mean force coefficients and the Strouhal number varying angle of attack, flow velocity and turbulence intensity. The experimental campaign mostly concerns the critical Re regime (in terms of effective Reynolds number of an equivalent circular cylinder), that can be of interest for real structures in serviceability conditions.

Main conclusions are summarized below.

- The drag coefficient (smooth flow) assumes values quite similar to those supplied by the literature for circular and multisided cylinders. However, the face-orientation produces the greatest drag force, differently from what is stated by current standards, which just consider the corner-orientation condition.
- The lift coefficient (smooth flow), which is usually not taken into account for such sectional shapes, is found to assume not negligible values for some angles of attack. This effect is mitigated increasing the corner radius, when the polygonal shape approaches the circular one. Considering the whole angle range 0°-360°, the variation of C_L seems quite erratic. This is however physically consistent for multi-

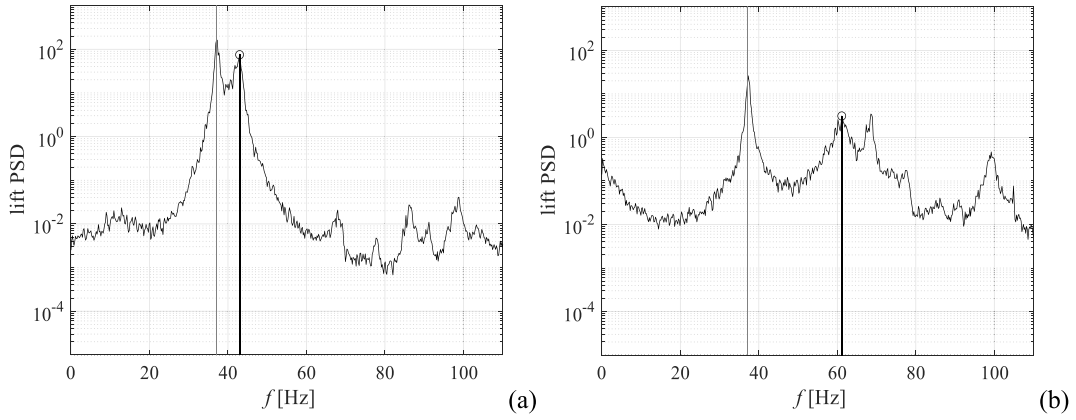

Fig. 17. Identification of vortex shedding frequency. Black vertical line indicates f_s, while grey lines identify the model frequencies. a) ū=13.6 m/s, smooth flow. b) ū=19.3 m/s, I_u = 7.5 %.

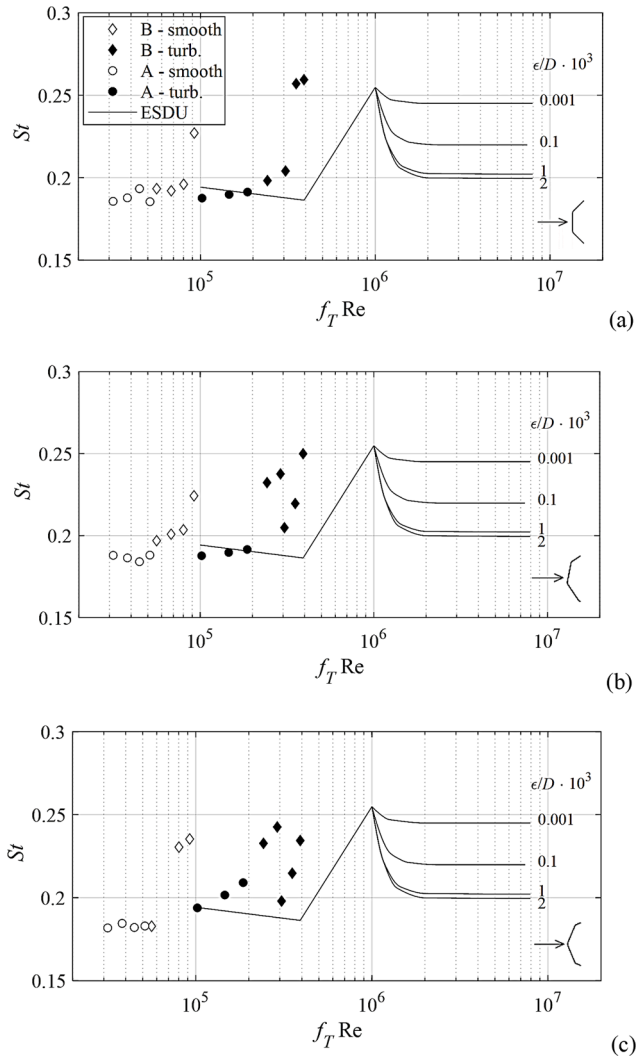

Fig. 18. Strouhal number as a function of effective Reynolds number for fixed angles of attack, measured and estimated by ESDU 96,030 [34]; a) $\alpha = 0°$ (face-orientation), b), $\alpha = 6°$ (mid-orientation), c) $\alpha = 11.25°$ (corner-orientation).

sided cylinder, where the C_L slopes are negative for flat orientation, and positive for corner orientation.

- The turbulence intensity drastically reduces drag coefficient values in agreement to the so-called effective Reynolds number, addressed by ESDU 79026. Concerning the lift coefficient, the presence of turbulence can reverse the sign of the C_L slopes, especially for low level of turbulence intensity (e.g., $I_u = 3.5$ %). Higher values of turbulence (e.g., $I_u = 7.5$ %) seem to mitigate this effect.
- Protuberances give rise to a CD and C_L increase when they are directly invested by the flow (upwind). Therefore, in the presence of imperfections or ancillaries along the pole (such as cables, ducts, etc.), provisions supplied by current standards can lead to underestimation of the aerodynamic loading. In the case under investigation, the effect of ladder seems particularly relevant, producing a strong increase of the aerodynamic coefficients in broad angular ranges that implies a regularization in the trend of the coefficients, especially concerning C_L.
- In smooth flow, by virtue of the observed behaviour of the lift coefficient in multisided cross sections, potential galloping conditions appears for a number of flow directions. The intensity of turbulence appears to change the potential critical angle of galloping with a weak mitigation for the highest turbulence value investigated. The ladder appears to have a strong effect on possible galloping conditions of the hexadecagonal cross-section, which shows stable behaviour for almost all angles measured.

Perspectives of this work are mainly divided in three research lines. It is planned to carry out dynamic wind tunnel tests to investigate the dynamic response of the cylinder, using a spring support system to describe the vortex shedding response [47–50] and possible galloping phenomena [51,52]. Such studies are fundamental for reliable assessment of the resistance and fatigue behaviour of many structural types [53–55]. In addition, the aerodynamic loading of non-stationary winds, such as thunderstorms, can be studied [56–58] introducing in the experiment typical effects induced by thunderstorms outflows [59]. Moreover, future work should be addressed to enhance the calibration of the turbulence factor f_T in order to obtain a better prediction of the drag coefficient for different flow and surface roughness.

CRediT authorship contribution statement

Andrea Orlando: Investigation, Validation, Data curation, Visualization, Writing – original draft. **Luisa Pagnini:** Methodology, Funding acquisition, Supervision, Writing – review & editing. **Maria Pia Repetto:** Conceptualization, Methodology, Funding acquisition, Supervision, Writing – review & editing.

Declaration of Competing Interest

The authors declare that they have no known competing financial interests or personal relationships that could have appeared to influence the work reported in this paper.

Data availability

Data will be made available on request.

Acknowledgements

The second and third authors acknowledge the support by the European Union's Horizon 2020 research and innovation program (ERC grant agreement No. 741273) for the project THUNDERR - Detection, simulation, modelling and loading of thunderstorm outflows to design wind safer and cost-efficient structures – that is carried out through an Advanced Grant 2016.

References

[1] Roshko A. On the wake and drag of bluff bodies. J Aero Sc 1955;22:124–32.
[2] Coutanceau M, Daefaye JR. Circular cylinder wake configurations: a flow visualization survey. Appl Mech Rev 1991;44(6):255–305.
[3] Williamson CHK. Defining a universal and continuous Strouhal-Reynolds number relationship for the laminar vortex shedding of a circular cylinder. Phys Fluids 1988;31(10):2742–4.
[4] Williamson CHK. Vortex dynamics in the cylinder wake. Ann Rev Fluid Mech 1996; 28:477–539.
[5] Zdravkovich MM. Flow around Circular Cylinders, Volume 1. Fundamentals: Oxford Science Publications; 1997.
[6] Thompson MC, Leweke T, Williamson CHK. The physical mechanism of transition in bluff body wake. J Fluids Struct 2001;15:607–16.
[7] Yeung WWH. On the relationships among Strouhal number, pressure drag, and separation pressure for blocked bluff-body flow. Trans ASME J Fluids Engng 2010; 132(2):021201.
[8] Okajima A. Strouhal numbers of rectangular cylinders. J Fluid Mech 1982;123: 379–98.
[9] Igarashi T. Drag reduction of a square prism by the flow control using a small rod. J Wind Eng Ind Aerodyn 1997;69(71):141–53.
[10] Matsumoto M. Vortex shedding of bluff bodies: a review. J Fluids Struct 1999;13: 791–811.
[11] Tamura T, Miyagi T. The effect of turbulence on aerodynamic forces on a square cylinder with various corner shapes. J Wind Eng Ind Aerodyn 1999;83:135–45.
[12] Breuer M, Bernsdor J, Zeiser T, Durst F. Accurate computations of the laminar flow past a square cylinder based on two different methods: lattice-Boltzmann and finite-volume. Int J Heat Fluid Flow 2000;21:186–96.

[13] Zhou L, Cheng M, Hung KC. Suppression of fluid force on a square cylinder by flow control. J Fluids Struct 2005;21:151–67.
[14] Van Hinsberg NP, Schewe G, Jacobs M. Experiments on the aerodynamic behaviour of square cylinders with rounded corners at Reynolds numbers up to 12 million. J Fluids Struct 2017;74:214–33.
[15] Van Hinsberg NP, Schewe G, Jacobs M. Experimental investigation on the combined effects of surface roughness and corner radius for square cylinders at high Reynolds numbers up to 10^7. J Wind Eng Ind Aerodyn 2018;173:14–27.
[16] Zuo D, Wu L, Smith DA, Morse SM. Experimental and analytical study of galloping of a slender tower. Eng Struct 2017;132:44–60.
[17] Kaczinski MR, Dexter RJ, Van Dien JP. Fatigue-resistant design of cantilevered signal, sign and light supports. Washington, D.C.: National Research Council, National Academy Press; 1998. NCHRP report 412. Transportation Research Board -.
[18] Letchford C, Cruzado HJ. Risk assessment model for wind-induced fatigue failure of cantilever traffic signal structures. Lubbock: Texas Tech University; 2007. Research Report 0–4586-4,.
[19] James WD. Wind Tunnel Tests of a Two-Dimensional Round-Cornered Dodecagonal Cylinder. Red Wing, MN: Meyer Manufacturing; 1971.
[20] James WD. Effects of Reynolds number and corner radius on two-dimensional flow around octagonal, dodecagonal and hexdecagonal cylinders. University of Iowa; 1976. PhD Dissertation,.
[21] James WD. Effects of Reynolds Number and Corner Radius on Two-Dimensional Flow Around Hexdecagonal Cylinders. In Proc AIAA Sixth Computational Fluid Dynamics Conference, Danvers, MA, American Institute of Aeronautics and Astronautics, Reston, VA; 1985.
[22] Mehta CK, Ritchie DL, Oler W. Wind drag coefficients for octagonal cylinders. Texas Technical University: Department of Highways and Public Transportation; 1990.
[23] Bosch HR, Guterres RM. Wind tunnel experimental investigation on tapered cylinders for highway support structures. J Wind Eng Ind Aerodyn 2001;89:1311–23.
[24] Aashto. Standard Specifications for Structural Supports for Highway Signs, Luminaires and Traffic Signals. American Association of State Highway and Transportation Officials; 1985.
[25] Tian X, Li S. Scientific measurements of disturbance on the prototype stands in a low speed wind tunnel. Exp Res Aerodyn 2007;25(3):1–6.
[26] Xu SJ, Zhang WG, Gan L, Li MG, Zhou Y. Experimental study of flow around polygonal cylinders. J Fluid Mech 2017;812:251–78.
[27] Tian ZW, Wu ZN. A study of two-dimensional flow past regular polygons via conformal mapping. J Fluid Mech 2009;628:121–54.
[28] Khaledi HA, Andersson HI. On vortex shedding from a hexagonal cylinder. Phys Lett A 2011;375(45):4007–21.
[29] CNR-DT 207 R1/2018. Guide for the assessment of wind actions and effects on structures. Rome, National Research Council of Italy; 2018.
[30] EN 1991-1-4. Eurocode 1: Actions on Structures – Part 1.4: General Actions – Wind Actions. CEN, European Committee for Standardization, Brussels, Belgium; 2005.
[31] ASCE/SEI 7-02. Minimum design loads for buildings and other structures. American Society of Civil Engineers; 2002.
[32] AASHTO LRFD Specifications for Structural Supports for Highway Signs, Luminaires, and Traffic Signals. American Association of State Highway and Transportation Officials; 2015.
[33] ESDU 79026. Mean fluid forces and moments on cylindrical structures: polygonal sections with rounded corners including elliptical shape. London, UK; 1980.
[34] ESDU 96030. Response of structures to vortex shedding. Structures of circular or polygonal cross section. London, UK; 1998.
[35] Nguyen CH, Freda A, Solari G, Tubino F. Aeroelastic instability and wind-excited response of complex lighting poles and antenna masts. Eng Struct 2015;85:264–76.
[36] Durgin FH, Palmer DA, White RW. The galloping instability of ice coated poles. J Wind Eng Ind Aerodyn 1992;41(1–3):675–86.
[37] Caracoglia L, Jones NP. Numerical and experimental study of vibration mitigation for highway light poles. Eng Struct 2007;29:821–31.
[38] Caracoglia L. Influence of weather conditions and eccentric aerodynamic loading on the large amplitude aeroelastic vibration of highway tubular poles. Eng Struct 2007;29(12):3550–66.
[39] Han Y, Zhou X, Wang L, Cai CS, Yan H, Hu P. Experimental investigation of the vortex-induced vibration of tapered light poles. J Wind Eng Ind Aerodyn 2021;211:104555.
[40] DeMello N, Smith J, Bridge JA, Consolazio GR, Gurley K. Investigation of aerodynamic shielding between traffic control attachments and mast-arm support structures. Eng Struct 2019;201:109784.
[41] Pulipaka N, Sarkar PP, McDonald JR. On galloping vibration of traffic signal structures. J Wind Eng Ind Aerodyn 1998;77&78:327–36.
[42] Achenbach E. Influence of surface roughness on the cross-flow around a circular cylinder. J Fluid Mech 1971:46 part 2:321-335.
[43] Szechenyi E. Supercritical Reynolds number simulation for two-dimensional flow over circular cylinders. J Fluid Mech 1975:70 part 3:529-542.
[44] Chang B, Sarkar P, Phares B. Time-Domain Model for Predicting Aerodynamic Loads on a Slender Support Structure for Fatigue Design. J Eng Mech 2010;136(6).
[45] Den Hartog JP. Mechanical Vibrations. 4th edition. New York, NY, USA: McGraw-Hill; 1956.
[46] Pagnini LC, Freda A, Piccardo G. Uncertainties in the evaluation of one degree-of-freedom galloping onset. Eur J Environ Civ En 2017;21(7–8):1043–63.
[47] Wang Q, Gan L, Xu S, Zhou Y. Vortex evolution in the near wake behind polygonal cylinders. Exp Therm Fluid Sci 2020;110:109940.
[48] Zuo D, Letchford CW. Wind-induced vibration of a traffic-signal-support structure with cantilevered tapered circular mast arm. Eng Struct 2010;32(10):3171–9.
[49] Pagnini LC, Piccardo G. A generalized gust factor technique for evaluating the wind–induced response of aeroelastic structures sensitive to vortex-induced vibrations. J Fluids Struct 2017;70:181–200.
[50] Pagnini LC, Piccardo G, Solari G. VIV regimes and simplified solutions by the spectral model description. J Wind Eng Ind Aerodyn 2020;198:104100.
[51] Joly A, Etienne S, Pelletier D. Galloping of square cylinders in cross-flow at low Reynolds numbers. J Fluids Struct 2012;28:232–43.
[52] Chen W, Zhao Y, Ji C, Srinil N, Song L. Experimental observation of flow-induced vibrations of a transversely oscillating D-section prism. Phys Fluids 2021;33:091701.
[53] Pagnini LC, Repetto MP. The role of parameter uncertainties in the damage prediction of the alongwind-induced fatigue. J Wind Eng Ind Aerodyn 2012;104–106:227–38.
[54] Repetto MP, Torrielli A. Long term simulation of wind-induced fatigue loadings. Eng Struct 2017;132:551–61.
[55] Tsai L-W, Alipour A. Studying the wind-induced vibrations of a traffic signal structure through long term health monitoring. Eng Struct 2021;247:112837.
[56] Letchford CW, Mans C, Chay MT. Thunderstorms - their importance in wind engineering (a case for the next generation wind tunnel). J Wind Eng Ind Aerodyn 2002;90:1415–33.
[57] Le V, Caracoglia L. Generation and characterization of a non-stationary flow field in a small-scale wind tunnel using a multi-blade flow device. J Wind Eng Ind Aerodyn 2019;186:1–16.
[58] Solari G, Burlando M, Repetto MP. Detection, simulation, modelling and loading of thunderstorm outflows to design wind-safer and cost-efficient structures. J Wind Eng Ind Aerodyn 2020;200:104142.
[59] Zhang S, Solari G, De Gaetano P, Burlando M, Repetto MP. A refined analysis of thunderstorm outflow characteristics relevant to the wind loading of structures. Prob Eng Mech 2018;54:9–24.